AAS 04-271

MARS EXPLORATION ROVER TERMINAL DESCENT MISSION MODELING AND SIMULATION

Behzad Raiszadeh*†, Eric M. Queen‡
NASA Langley Research Center, Hampton VA

ABSTRACT

Because of NASA's added reliance on simulation for successful interplanetary missions, the MER mission has developed a detailed EDL trajectory modeling and simulation. This paper summarizes how the MER EDL sequence of events are modeled, verification of the methods used, and the inputs. This simulation is built upon a multibody parachute trajectory simulation tool that has been developed in POST II that accurately simulates the trajectory of multiple vehicles in flight with interacting forces. In this model the parachute and the suspended bodies are treated as 6 Degree-of-Freedom (6 DOF) bodies. The terminal descent phase of the mission consists of several Entry, Descent, Landing (EDL) events, such as parachute deployment, heatshield separation, deployment of the lander from the backshell, deployment of the airbags, RAD firings, TIRS firings, etc. For an accurate, reliable simulation these events need to be modeled seamlessly and robustly so that the simulations will remain numerically stable during Monte-Carlo simulations. This paper also summarizes how the events have been modeled, the numerical issues, and modeling challenges.

INTRODUCTION

The MER mission design during the terminal descent phase borrows many elements from previous successful Mars exploration missions. Terminal descent phase is the period starting from parachute deployment to first ground impact. In modeling the terminal descent phase, an attempt has been made to use some of the same modeling techniques and assumptions as in previous Mars lander mission simulations. Parachute design and method of deployment draw heritage from past missions. In the parachute deployment event, the simulation transitions from a single vehicle in flight to a multiple vehicle simulation.

After the parachute is deployed, a sequence of events must take place for a successful landing. Twenty seconds after mortar fire, at heatshield jettison, six pre-compressed springs push the heatshield away from the rest of the entry capsule. Deployment of the lander from the backshell begins ten seconds after heatshield release. The lander is lowered from the backshell using the Descent Rate Limiter (DRL). The main function of the DRL is to reel the lander away from the

* Mail Stop 365, E-mail: b.raiszadeh@larc.nasa.gov, Tel: (757) 864-1050
† This author has also published papers under the name Ben Raiszadeh.
‡ Mail Stop 365, E-mail: e.m.queen@larc.nasa.gov, Tel: (757) 864-6610

backshell smoothly, thus reducing the loads on the system during such maneuver. The Rocket Assisted Descent (RAD) rocket motors are commanded to ignite at a time determined by the on-board flight software. In an ideal scenario the RAD rocket motors reduce the rate of descent to zero at the end of the burn at a safe height above ground. The airbags are inflated just before the RAD rockets fire. Because of the large payload mass, the airbags are more vulnerable to rupture at high grazing angles. To reduce this vulnerability, Transverse Impulse Rocket Subsystem (TIRS) has been included in MER. These TIRS rockets are controlled by the onboard computer which uses the rockets to reduce the grazing angle at impact. The TIRS algorithm must estimate the attitude, and relative position and velocity of the lander and backshell to compute the best TIRS firing solution. Because this algorithm is sensitive to the exact attitudes and positions of both lander and backshell, a great deal of emphasis has been placed on detailed terminal descent multibody trajectory simulation.

The current simulation includes detailed models of parachute deployment, heatshield release, lander deployment, RAD and TIRS firings, and includes flight software in the loop.

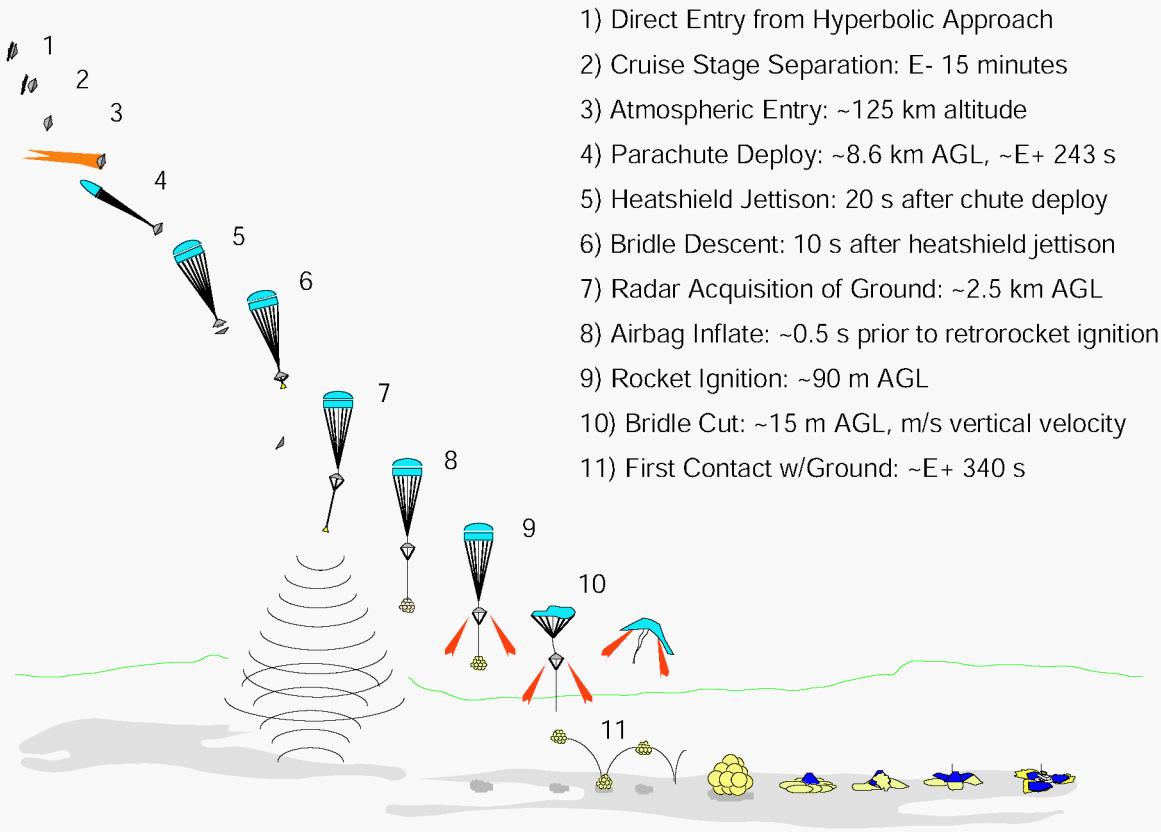

Figure 1 MER Sequence of Events

EDL EVENTS

Parachute Deployment

The MER parachute deployment time is determined by the onboard computer, designed to open the parachute at appropriate flight conditions. A detailed discussion of MER parachute deployment is discussed in Reference 4. Prior to parachute deployment, the vehicle is modeled as one six-degree-of-freedom vehicle. At the moment of parachute deployment, the simulation transitions to two 6 DOF bodies and one 3 DOF body (15 DOFs total). The parachute is treated as a rigid 6 DOF body and the confluence point is treated as a 3 DOF body with a small mass (Figure 2).

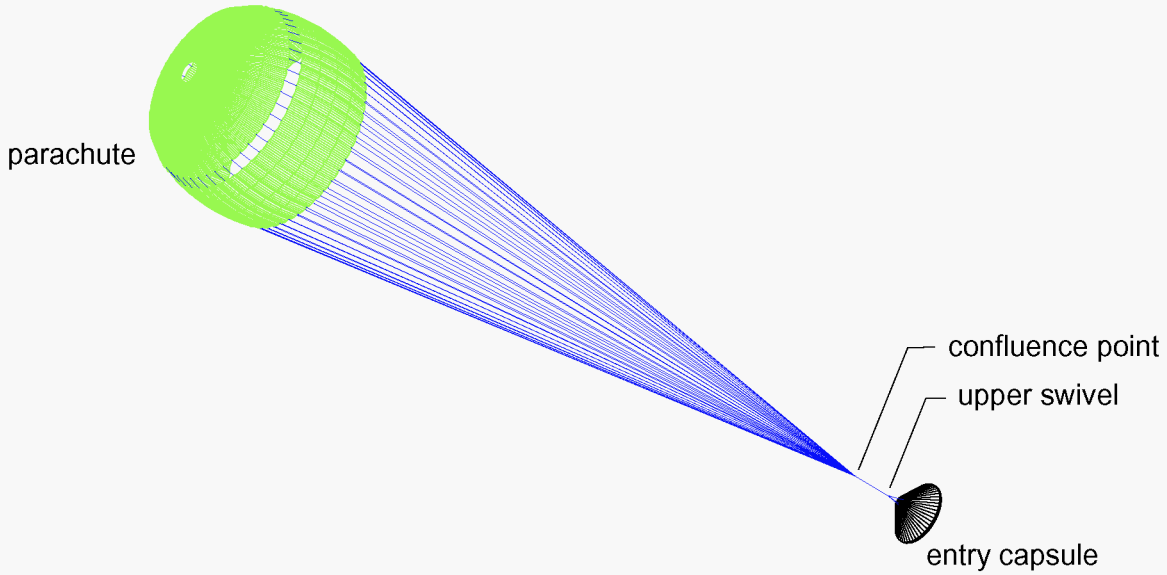

Figure 2 Configuration After Parachute Deploy

Nominally the parachute is ejected at a rate of 37.9 m/s relative to the entry capsule. In the simulation, it is assumed that a constant force applied over a period of 0.1 second accelerates the parachute away from the entry capsule. A force that is equal in magnitude and opposite in directions is applied to both bodies. The applied force is found using the following relationships:

$I = m\Delta v$ Impulse is equal to the product of mass and change in velocity

$I = F\Delta t$ Impulse is also equal to area under the force profile

$F = \frac{m\Delta v}{\Delta t}$ Constant mortar force

$$F = \frac{14.63 \times 37.9}{0.1} = 5545N$$

It is assumed that the MER parachute takes 1.3 seconds after the mortar fire to fully inflate. The parachute inflation profile is shown in Figure 3.

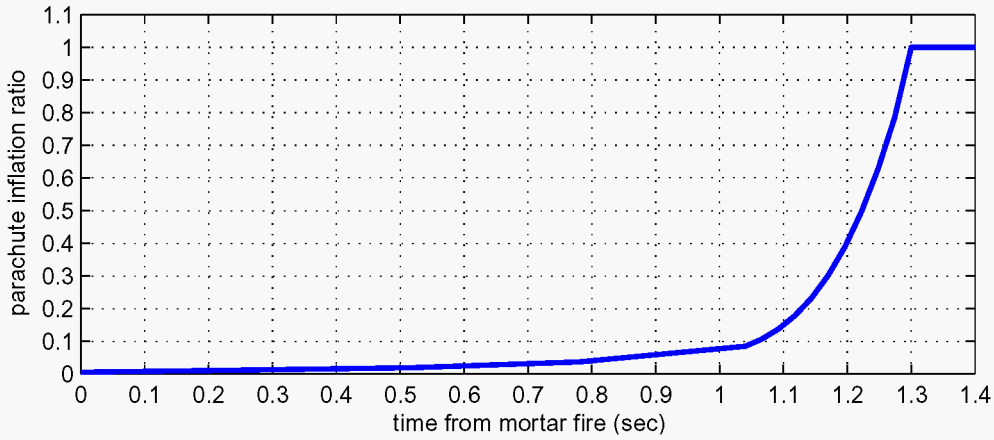

Figure 3 Parachute Inflation Profile

Parachute inflation ratio of 1.0 corresponds to full inflation. In the simulation, the parachute aerodynamic properties are scaled by to the parachute inflation ratio during inflation. Figure 4 shows the parachute force on the entry capsule during parachute deployment for a nominal MER simulation. Note that there are two peaks in the force profile. The first peak, referred to as the "snatch load", is the inertial force experienced by the capsule when the parachute mass gets to the end of the line. The second peak, known as the "opening load", occurs as the parachute is nearly inflated and the entry capsule deceleration is at the maximum value. In flight tests, the "snatch load" tends to be smaller in magnitude. The relatively high "snatch load" here is due to modeling assumption. In reality, the center of mass of the parachute, which includes the suspension lines, moves backward in a more gradual fashion, so the "snatch load" is not as severe.

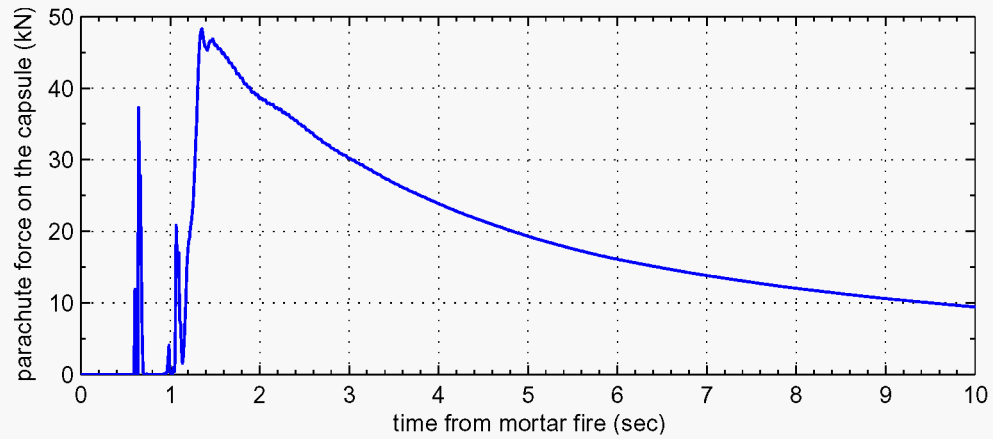

Figure 4 Parachute Force

Heatshield Separation

The heatshield separation event occurs 20 seconds after mortar fire. The separation mechanism consists of six pre-compressed springs spaced symmetrically around the entry capsule outer diameter between the heatshield and the backshell (Figure 5). In the end-to-end MER simula-

tion, the heatshield motion is not simulated after separation. However, it is desired that the IMU model, embedded in the simulation, record the accelerations due to separation forces.

The separation springs are assumed to behave like ideal springs as they relieve their stored compressive energy. Because of symmetry, it is reasonable to assume that all motion occurs in the axial direction. This simplifies the system to a dynamic system with two masses connected by a spring with each mass having one degree of freedom. The spring stiffness in the simplified model would have six times the stiffness of one spring.

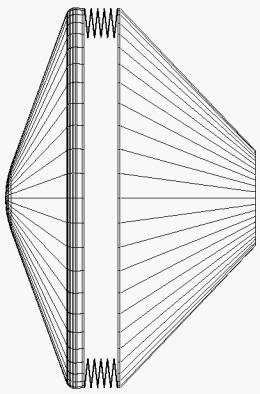

Figure 5 Separation Springs

The motion of the simplified system can be described by two, second order differential equations. The details of solving the differential equations are not discussed here. But, in summary, the system can be reduced to a linear system of four, first order differential equations. Solution to such a system can be found in most introductory dynamics textbooks. The following is the summary of the inputs used along with the resulting force profile (Figure 6). This force profile is applied to the backshell in the POST II multibody simulation.

Table 1
SEPARATION SPRING PARAMETERS

Parameter	**Value**
Backshell/lander mass (MER-A)	720.665 Kg
Heatshield mass (MER-A)	89.6 kg
Spring stiffness per spring	10874.8 N/m
Stroke length	0.0762 m

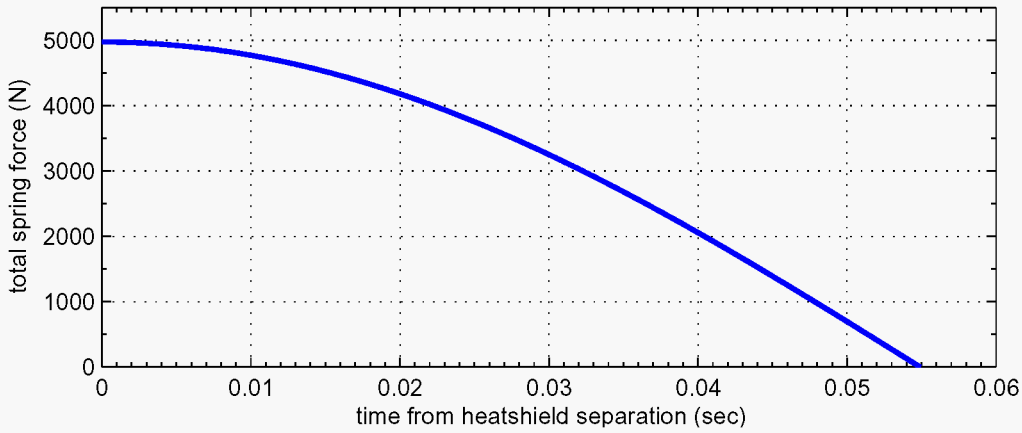

Figure 6 Separation Spring Force Profile

In the POST II simulation a third of the above force is applied at 3 locations axisymmetrically around the outer edge of the backshell/heatshield interface.

DRL Deployment

After heatshield separation, the next major event is the deployment of the lander from the heatshield using the Descent Rate Limiter (DRL). A detailed description of the DRL and its operation is given in Reference 5. A summary is presented here for completeness. The lander separation event occurs ten seconds after heatshield jettison. At the start of the lander separation/DRL deployment event, the POST II simulation transitions from three-body to a five-body simulation. The properties of the parachute and the upper swivel remain unchanged. However the backshell/lander combination is split into three bodies, the backshell, the lander, and the lower swivel (Figure 7). The locations of center of masses for all the vehicles are adjusted based on the best estimates for their locations at the start of lander separation.

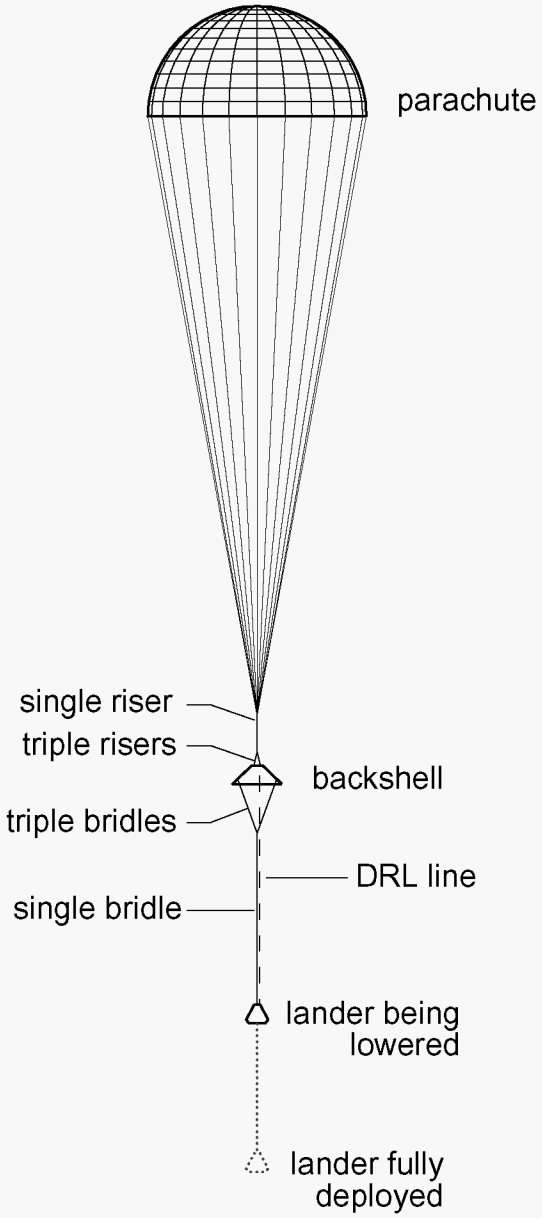

Figure 7 Configuration After Lander Separation

The DRL used for MER is based on a centrifugal braking mechanism. The main purpose of the DRL is to reduce dynamic loading of the lander during the lowering maneuver. The DRL device is rigidly attached to the petals with the DRL line wound around the drum. The fixed end of the DRL line is attached to the backshell. In the simulation, the DRL remains active until the single bridle is loaded. The DRL damping force is proportional to the square of the velocity of separation. The damping force is given by:

$$F_{drl} = \frac{c\dot{d}}{R^3}$$

R is a function of backshell/lander separation (d) as described in Reference 5.

$$R(d) = R_0\sqrt{1-\left(1-\frac{R_1^2}{R_0^2}\right)\left(\frac{d-s}{L-s}\right)}$$

where,

F_{drl}	DRL damping force
c	Mechanical constant related to the mechanism design
R	Drum radius
d	Distance between the two ends of the DRL line
$\dot{d}$	Descent rate
L	Total length of the DRL line
s	Initial DRL line slack
R_0	Initial drum radius
R_1	Final drum radius

The nominal values of the DRL parameters are listed in Table 2. Figure 8 shows the force profile experienced by the DRL line in a nominal case.

Table 2
DRL INPUT PARAMETERS

Input Parameter	Value
R_0	0.0254 m
R_1	0.0254 m
C	0.0032 N-m-sec^2
S	0.0100 m
L	19.771 m

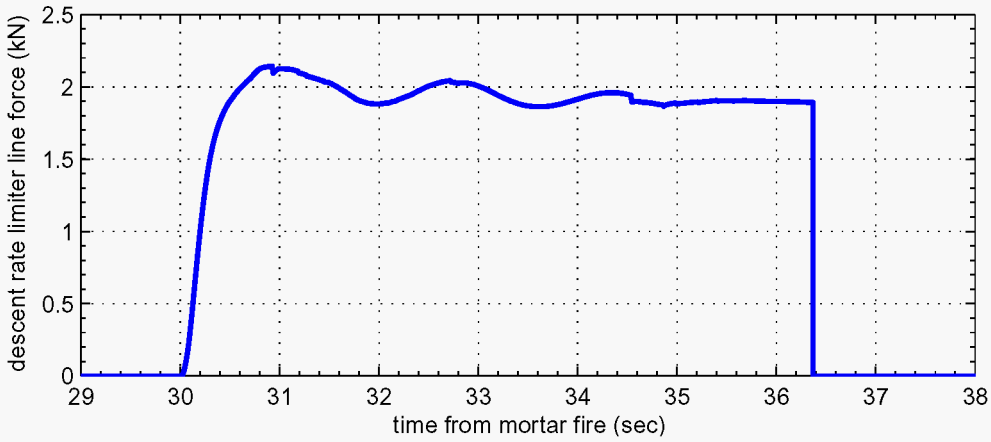

Figure 8 Descent Rate Limiter Line Force

Airbag Deployment

The airbag deployment is modeled as an instantaneous event. In MER mission time-line, air-bag deployment occurs on a timer half a second before the RAD firing event. In the POST II terminal descent simulation, the aerodynamic properties of the lander are changed at this event to reflect changes in aerodynamic properties, and the moments of the inertia are also changed to account for the change in the mass distribution.

RAD Firing

Three RAD rockets are placed axisymmetrically around the centerline of the backshell. The direction of thrust of each motor is approximately 28° away from the backshell centerline (Figure 9). The time of RAD firing is determined by the flight software. This time is chosen with several parameters factored in. The detail discussion of RAD algorithm is out of scope of this paper. The RAD rockets continue reducing the lander's rate of descent until the bridle connecting the backshell and the lander is severed (bridle-cut event). Time to cut the bridle is also determined by the onboard flight software. The bridle-cut time calculated by the flight software is such that not all the fuel is spent at bridle-cut, so the remainder of the burn carries the backshell and parachute safely away from the lander.

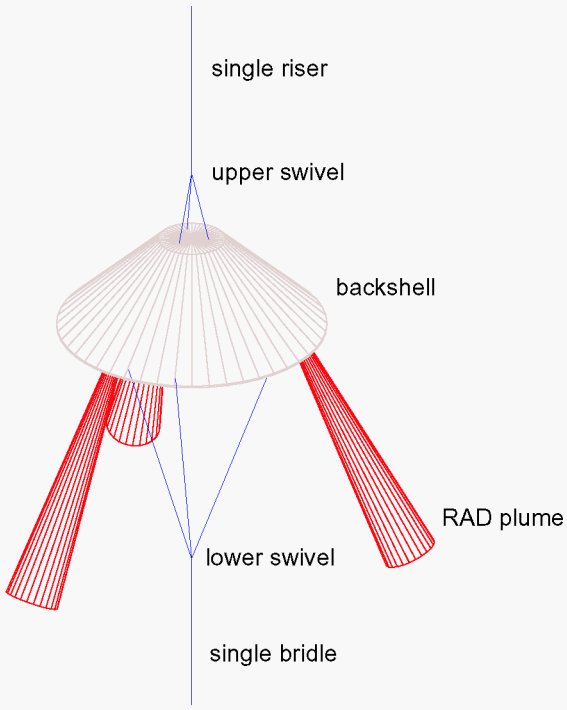

Figure 9 RAD Configuration

Parachute Offloading

Just prior to RAD ignition the parachute exerts a considerable force on the backshell. However, starting at RAD ignition, the parachute pull on the backshell gradually begins to diminish. In most cases, the parachute is completely offloaded during the RAD burn. The flight software predicts the offloading of the parachute in order to come up with a good solution for when to initiate RAD rockets and when to cut the bridle. Mass of the parachute does not account for all the inertial forces which influence the dynamics of the parachute. Mass of the entrained air should also be included in the simulations. The entrained air mass needs to be treated separately from the mass of the parachute. The entrained air mass resists being accelerated, however it is not subject to gravitational forces.

Figure 10 illustrates the effects of the entrained air mass on parachute offloading for the nominal MER trajectory simulation run. Note that due to dynamical nature of the problem, the parachute does not offload smoothly, rather it exhibits an oscillatory behavior. The added inertia of the entrained air causes the parachute deceleration rate to be smaller, hence causing the parachute to drop and offload more rapidly.

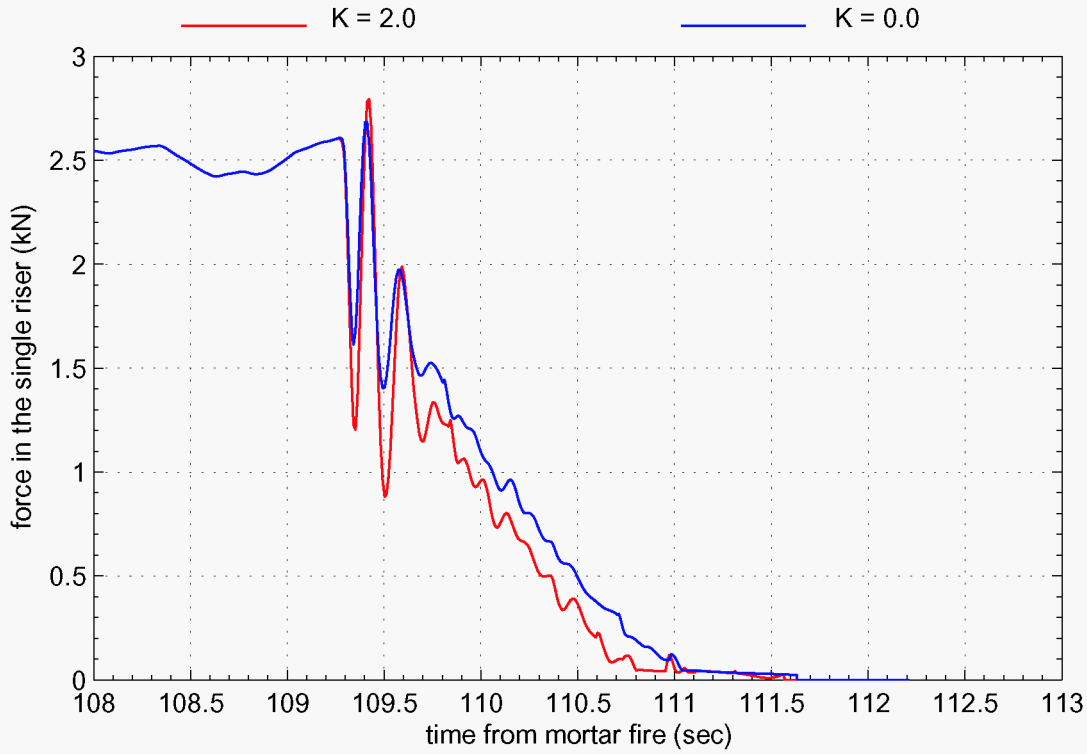

Figure 10 Parachute Offloading

In the simulation, the entrained air mass effects are modeled by applying the resultant inertial force on the parachute.

Nomenclature:

m_e	Entrained air mass
m_p	Parachute mass
$\vec{F}_{ext}$	All external forces acting on the parachute except the force of gravity
$\vec{F}_e$	Force due to entrained air mass
m_e	Entrained air mass
$\vec{a}$	Acceleration due to all external forces except the force of gravity

Derivation:

$$\sum \vec{F} = m_p \vec{a}$$

$$\vec{F}_{ext} + \vec{F}_e = m_p \vec{a}$$

$$\vec{F}_{ext} - m_e \vec{a} = m_p \vec{a}$$

$$\vec{a} = \frac{\vec{F}_{ext}}{m_p + m_e}$$

$\vec{F}_e = -m_e \vec{a}$ Entrained air mass force is opposite of acceleration

$\vec{F}_e = -\frac{m_e}{m_p + m_e} \vec{F}_{ext}$ The right hand side parameters on are available at every time step

In the POST II simulation this force is calculated at every time step and applied to the parachute in the direction opposite to the direction of the external forces.

RESULTS

Figure 11 shows the single riser force time history for a nominal run. Events have been annotated for clarity. Note the disturbance caused in the single riser force when the single bridle is first loaded during lander separation maneuver. Unloading of the single riser during RAD firing is also apparent in this plot. Figure 12 shows the force time history of the single bridle line. The single bridle line vibrates considerably at first when the lander is deployed. The next major disturbance occurs during the RAD rocket firings. At this event, the RAD thrust force is transferred to the lander through the single bridle line.

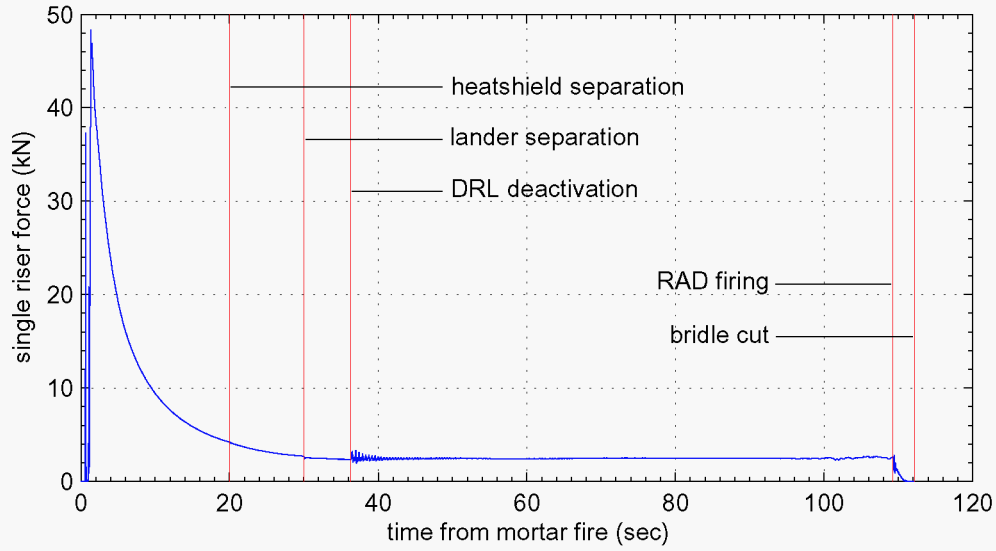

Figure 11 Single Riser Force Profile

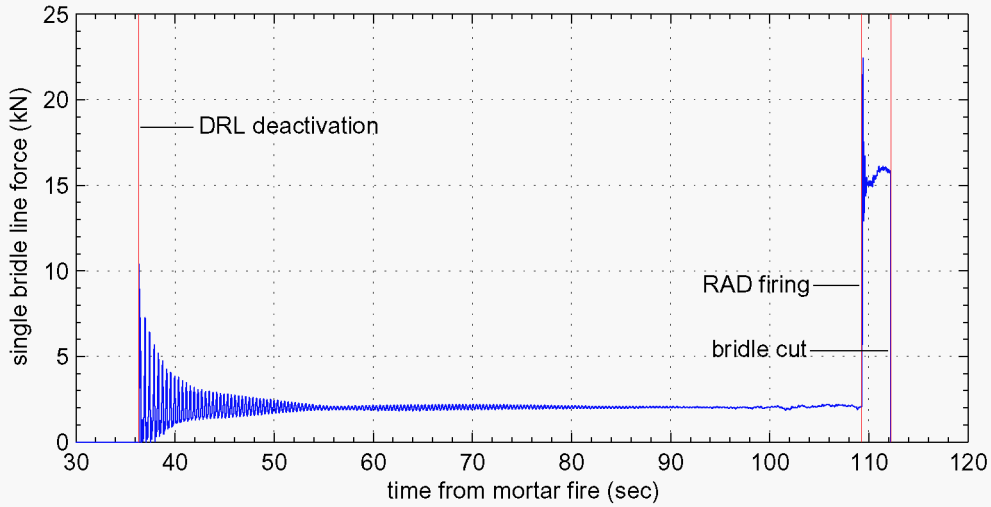

Figure 12 Single Bridle Force Profile

Figure 13 shows the backshell total angle of attack profile starting at deployment of the parachute. Angle of attack of the backshell tends to follow the parachute's trim angle of attack. The triple risers keep the parachute and the backshell in the same axial direction, in effect stabilizing the backshell. The high angle of attack during lander deployment is due to the fact that the DRL attach point is about 20 centimeters away from the centerline of the parachute, exerting a considerable about of torque during the lander deployment event.

Figure 14 shows the backshell angle of attack and the sideslip angle time history profiles. The overall sinusoidal nature of the curve is due to the fact that the parachute is coning.

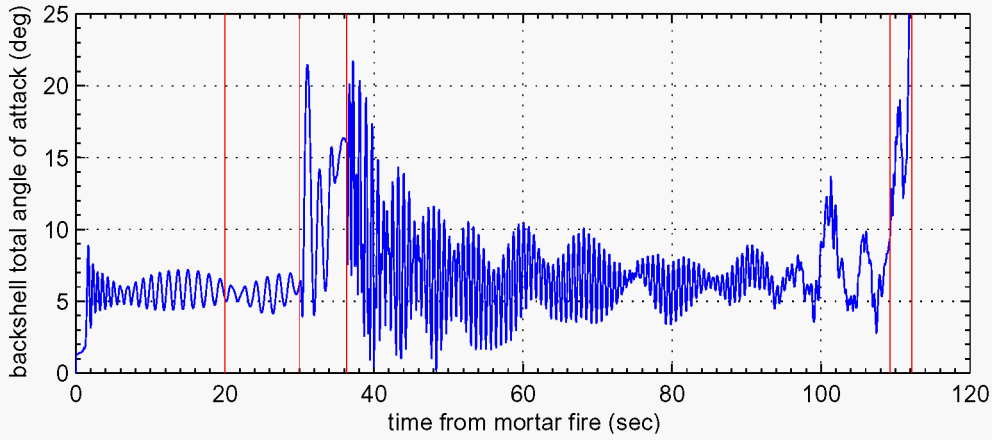

Figure 13 Backshell Total Angle of Attack

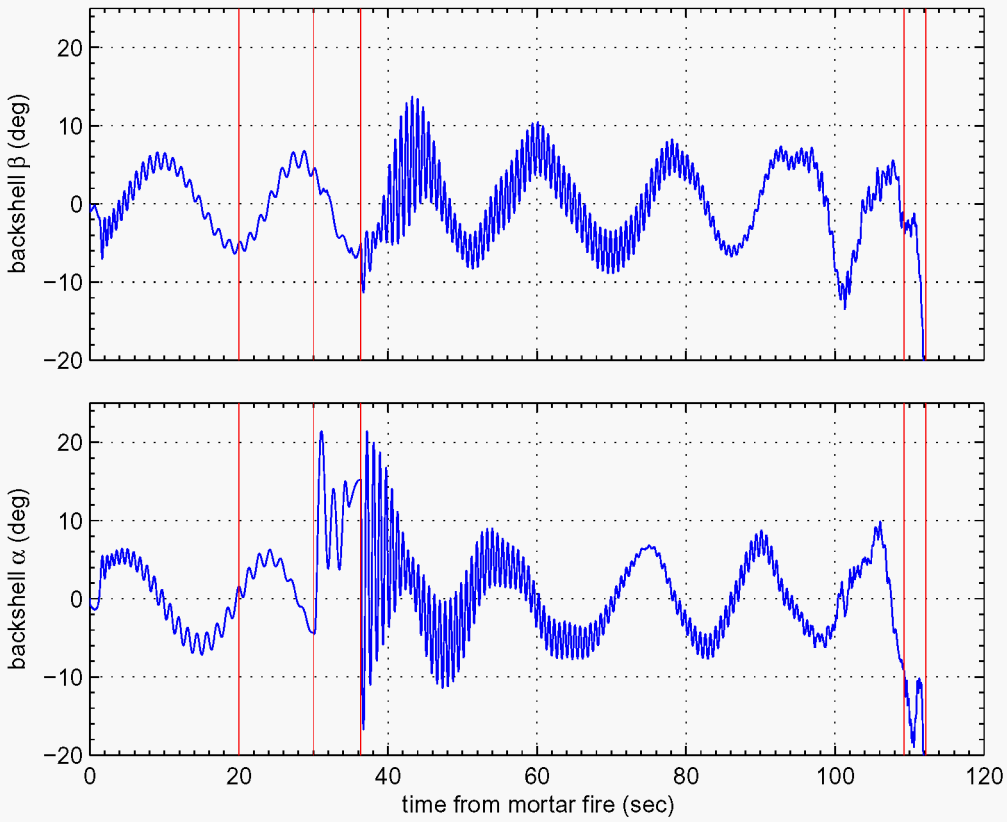

Figure 14 Backshell Angle of Attack and the Sideslip Angle

CONCLUSIONS

The MER multibody capability in POST II was used as the prime simulation tool on the MER project for Entry, Descent, Landing. The EDL team used the simulation to tune the flight control parameters. Success of the mission depended on the onboard flight computer system making proper decisions on when to fire the RAD rocket, whether to activate the TIRS system, and if so, which TIRS motor(s) to fire, and when to cut the bridle. By running thousands of cases with varying winds and atmospheric conditions in the Monte-Carlo simulations, the EDL team was able to make the control system more robust, such that it is able to respond appropriately in the harsh Mars environments.

ACKNOWLEDGEMENT

Many members of the MER EDL team have made contributions to the multibody simulation in POST II. The authors would like to give special thanks to Wayne Lee, Rob Grover, Robert Mitcheltree, Chia-Yen Peng, Erik Bailey, and Adam Steltzner all from JPL, and Prasun Desai, Juan Cruz, and Mark Schoenenberger of NASA Langley Research Center.

ACRONYMS

AGL	Above Ground Level
DOF	Degree of Freedom
DRL	Descent Rate Limiter
EDL	Entry, Descent, Landing
IMU	Inertial Measurement Unit
MER	Mars Exploration Rover
POST	Program to Optimize Simulated Trajectories
RAD	Rocket Assisted Descent
TIRS	Transverse Impulse Rocket Subsystems

REFERENCES

[1] Behzad(Ben) Raiszadeh, Validation of Multibody Program to Optimize Simulated Trajectories II (POST II) Parachute Simulation With Interacting Forces, Master Thesis, George Washington University, May 2004.

[2] Behzad(Ben) Raiszadeh, Eric M. Queen, Partial Validation of Multibody Program to Optimize Simulated Trajectories II (POST II) Parachute Simulation With Interacting Forces, NASA/TM-2002-211634, April 2002.

[3] Eric M. Queen, Behzad(Ben) Raiszadeh, Mars Smart Lander Parachute Simulation Model, AIAA Paper 2002-4616, August 2002.

[4] Prasun N. Desai, Mark Schoenenberger, F.M. Cheatwood, Mars Exploration Rover Six-Degree-Of-Freedom Entry Trajectory Analysis, Presented in AAS/AIAA Astrodynamics Specialists Conference, Big Sky Montana, August 3-7 2003.

[5] Kenneth S. Smith, Chia-Yen Peng, Ali Behboud, Multibody Dynamic Simulation of Mars Pathfinder Entry, Descent and Landing, JPL D-13298, April 1995.

[6] Program to Optimize Simulated Trajectories: Volume II, Utilization Manual, prepared by: R.W. Powell, S.A. Striepe, P.N. Desai, P.V. Tartabini, E.M. Queen; NASA Langley Research Center, and by: G.L. Brauer, D.E. Cornick, D.W. Olson, F.M. Petersen, R. Stevenson, M.C. Engel, S.M. Marsh; Lockheed Martin Corporation, Version 1.1.1.G, May 2000.